A RATIONAL LENGTH SCALE FOR LARGE-EDDY SIMULATIONS ON ANISOTROPIC GRIDS

F.X.Trias¹, J.Ruano¹, E.Di Lavore¹, A.Duben², A.Gorobets²

¹ Heat and Mass Transfer Technological Center, Technical University of Catalonia, c/Colom 11, 08222 Terrassa, Spain

² Keldysh Institute of Applied Mathematics, 4A, Miusskaya Sq., Moscow 125047, Russia francesc.xavier.trias@upc.edu

Abstract

Direct numerical simulation of turbulence is too costly for most practical cases, making dynamically simplified formulations like eddy-viscosity LES models widely used in both academia and industry. These models require a subgrid characteristic length, typically related to the local grid size. While its definition is straightforward for isotropic meshes, determining an appropriate length scale for unstructured or anisotropic Cartesian meshes, such as the pancakelike meshes commonly used to capture near-wall turbulence or shear layers, remains a challenge. In this work, we propose a novel subgrid length derived from the interplay between numerical discretization and filtering in LES. Its favorable mathematical properties and simplicity make it well-suited to reduce the impact of mesh anisotropies. Its effectiveness is demonstrated through simulations of decaying isotropic turbulence and turbulent channel flow.

1 Introduction

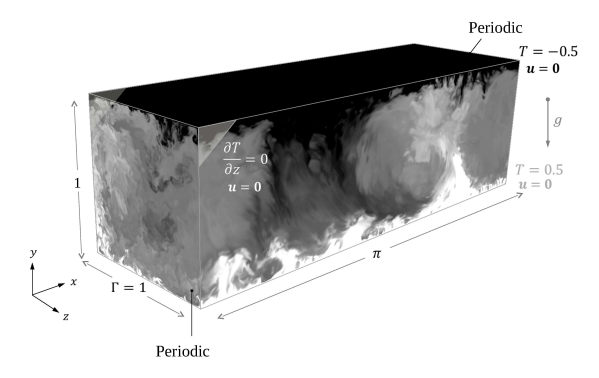
Direct numerical simulations (DNS) of the Navier–Stokes (NS) equations remain impractical for most real-world turbulent flows because not enough resolution is available to resolve all the relevant scales (see examples in Figure 1). Therefore, practical simulations have to resort to turbulence modeling. Hence, we may turn to large-eddy simulation (LES) to predict the large-scale behavior of turbulent flows: namely, the large scales are explicitly computed, whereas effects of small scale motions are modeled. LES equations result from applying a spatial commutative filter, with filter length δ , to the NS equations

$$\partial_t \overline{\boldsymbol{u}} + (\overline{\boldsymbol{u}} \cdot \nabla) \, \overline{\boldsymbol{u}} = \nu \nabla^2 \overline{\boldsymbol{u}} - \nabla \overline{p} - \nabla \cdot \tau(\overline{\boldsymbol{u}}), \quad \nabla \cdot \overline{\boldsymbol{u}} = 0,$$
(1)

where \overline{u} is the filtered velocity and $\tau(\overline{u})$ is the subgrid stress (SGS) tensor and aims to approximate the effect of the under-resolved scales, $\tau(\overline{u}) \approx \overline{u} \otimes \overline{u} - \overline{u} \otimes \overline{u}$. Because of its inherent simplicity and robustness, the eddy-viscosity assumption is by far the most used closure model, i.e. $\tau(\overline{u}) \approx -2\nu_t S(\overline{u})$. Then, the eddy-viscosity, ν_t , is usually modeled as follows

$$\nu_t = (C_m \delta)^2 D_m(\overline{\boldsymbol{u}}),\tag{2}$$

where C_m is the model constant, δ denotes the sub-



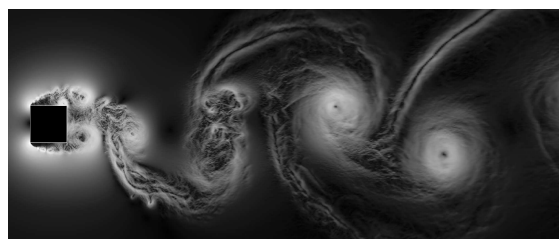


Figure 1: Two examples of DNS simulations are shown. Top: an air-filled (Pr=0.7) Rayleigh–Bénard configuration studied by Dabbagh et al. (2020), at Rayleigh numbers up to $Ra=10^{11}$. The highest Ra was computed on 8192 CPU-cores of the MareNostrum 4 supercomputer using a mesh with 5.7 billion grid points. Bottom: a turbulent flow around a square cylinder at Re=22000, analyzed in Trias et al. (2015b), computed on 784 CPU-cores of MareNostrum 3 supercomputer with a mesh of 323 million grid points.

grid characteristic length, and $D_m(\overline{u})$ is the model-specific differential operator, with units of frequency. The length scale δ , is the responsible for capturing the effective cut-off length scale, *i.e.* the spatial scale that separates the resolved turbulent motions, \overline{u} , from the unresolved ones in an LES simulation. Then, the rest of the flow physics, such as the forward/backward scattering, laminar-to-turbulence transitions, 2D flow behavior or presence of walls must be captured by the the differential operator that defines the SGS model, *i.e.* $D_m(\overline{u})$.

In the last decades, most of the research has focused on either the calculation of the model constant, C_m

(e.g. the dynamic modeling approach and its variants), or the development of more appropriate model operators $D_m(\overline{u})$ (e.g. WALE, Vreman's, Verstappen's, σ -model, S3PQR,...). Surprisingly, little attention has been paid on the computation of the subgrid characteristic length, δ . Due to its simplicity and applicability to unstructured meshes, the approach proposed by Deardorff (1970), i.e. the cube root of the cell volume (see Eq. 4), is by far the most widely used to computed the δ , despite in some situations it may provide very inaccurate results.

Alternative methods to compute δ are summarized and classified in Table 1 according to a list of desirable properties for a (proper) definition of δ . According to the property **P3**, they can be classified into two main families; namely, (i) definitions of δ that solely depend on geometrical properties of the mesh, and (ii) definitions of δ that are also dependent on the local flow topology. The latter is characterized by the gradient of the resolved velocity field, $G \equiv \nabla \overline{u}$, whereas the local mesh geometry for a Cartesian grid is contained in the following second-order diagonal tensor,

$$\Delta \equiv \operatorname{diag}(\Delta x, \Delta y, \Delta z). \tag{3}$$

The first seven definitions listed in Table 1 are given by

$$\delta_{\text{vol}} = (\Delta x \Delta y \Delta z)^{1/3}, \quad \delta_{\text{Sco}} = f(a_1, a_2) \delta_{\text{vol}}, \quad (4)$$

$$\delta_{\max} = \max(\Delta x, \Delta y, \Delta z),\tag{5}$$

$$\delta_{\omega} = \sqrt{\frac{\omega_x^2 \Delta y \Delta z + \omega_y^2 \Delta x \Delta z + \omega_z^2 \Delta x \Delta y}{|\omega|^2}}, \quad (6)$$

$$\tilde{\delta}_{\omega} = \max_{n,m} \frac{|\boldsymbol{l}_n - \boldsymbol{l}_m|}{\sqrt{3}}, \ \delta_{\text{SLA}} = \tilde{\delta}_{\omega} F_{\text{KH}}(VTM)$$
 (7)

$$\delta_{\text{lsq}} = \sqrt{(\hat{\mathsf{G}}\hat{\mathsf{G}}^T : \mathsf{G}\mathsf{G}^T)/(\mathsf{G}\mathsf{G}^T : \mathsf{G}\mathsf{G}^T)},\tag{8}$$

where $\omega = \nabla \times \boldsymbol{u}$ is the vorticity and $f(a_1, a_2) = \cosh \sqrt{4/27}[(\ln a_1)^2 - \ln a_1 \ln a_2 + (\ln a_2)^2]$ is the correcting function proposed by Scotti et al. (1993). The function $0 \leq F_{\rm KH}(VTM) \leq 1$ was proposed by Shur et al. (2015) to correct the $\tilde{\delta}_{\omega}$ definition proposed by Mockett et al. (2015) in shear layers. Both definitions were proposed in the context of Detached Eddy Simulation (DES). Finally, $\hat{\mathsf{G}} \equiv \mathsf{G}\Delta$ is the gradient in the so-called computational space. These properties are based on physical, numerical, and practical arguments. The list is completed with the new definitions $\delta_{\rm rls}$ and $\tilde{\delta}_{\rm rls}$ derived below.

2 Finite-volume filtering

Let us consider a generic 1D convection-diffusion equation

$$\frac{\partial \phi}{\partial t} + \frac{\partial (u\phi)}{\partial x} = \frac{\partial}{\partial x} \left(\Gamma \frac{\partial \phi}{\partial x} \right), \tag{9}$$

where u(x,t) denotes the advective velocity and $\phi(x,t)$ represents a generic (transported) scalar field.

	$\delta_{ m vol}$	$\delta_{ m Scc}$	$\delta_{ m ma}$	$_{ m x}\delta_{m{\omega}}$	$ ilde{\delta}_{m{\omega}}$	δ_{SL}	$_{ m A}\delta_{ m lsq}$	$\delta_{ m rls}$	$ ilde{\delta}_{ m rls}$
Eq.	(4)	(4)	(5)	(6)	(7)	(7)	(8)	(15)	(18)
P1	Y Y N N Y	Y	Y	Y	Y	Y	Y	Y	Y
P2	Y	Y	Y	Y	Y	N	Y	Y	Y
P3	N	N	N	Y	Y	Y	Y	\mathbf{Y}^c	Y
P4	Y	N	N^a	N^b	Y	Y	Y	Y	Y
P5	N	N	N	N	N	N	N	Y	N
P6	+	+	+	++	+++	++++	+++	+	+++
P7	+	+	+	++	++	+++	+++	+	+++

Table 1: Properties of different definitions of the subgrid characteristic length, δ . Namely, **P1**: $\delta \geq 0$, locality and frame invariant; **P2**: boundedness, *i.e.*, given a structured Cartesian mesh where $\Delta x \leq \Delta y \leq \Delta z$, $\Delta x \leq \delta \leq \Delta z$; **P3**: sensitive to flow orientation; **P4**: applicable to unstructured meshes; **P5**: directly computed at the cell faces; **P6**: computational cost; **P7**: memory footprint. ^a Possible with some adaptations; ^b a generalization for unstructured meshes was proposed by Deck (2012); ^c $\delta_{\rm rls}$ is computed at the faces independently of the local flow field, however, its effect ultimately depends on it.

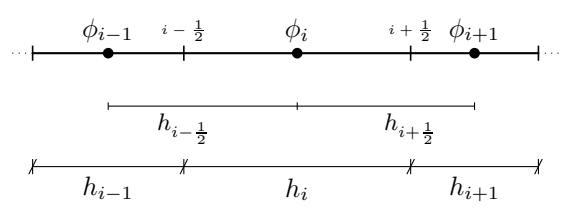


Figure 2: One-dimensional mesh

In the finite-volume method (FVM), this equation is integrated over a set of non-overlapping volumes. Hence, FVM variables result by applying a box filter with filter width equal to the local grid size, h,

$$\overline{\phi}(x) = \frac{1}{h} \int_{x-\frac{h}{2}}^{x+\frac{h}{2}} \phi dx. \tag{10}$$

Notice that this filter commutes with differentiation

$$\frac{\partial \overline{\phi}}{\partial x} = \frac{1}{h} \frac{\partial}{\partial x} \int_{x - \frac{h}{2}}^{x + \frac{h}{2}} \phi dx = \frac{1}{h} \int_{x - \frac{h}{2}}^{x + \frac{h}{2}} \frac{\partial \phi}{\partial x} dx = \frac{\overline{\partial \phi}}{\partial x}.$$
(11)

Moreover, the standard second-order approximation of the first-derivative at the face is exactly equal to the filtered derivative

$$\frac{\partial \phi}{\partial x}\Big|_{i+\frac{1}{2}} \approx \frac{\phi_{i+1} - \phi_i}{h_{i+\frac{1}{2}}} = \frac{1}{h_{i+\frac{1}{2}}} \int_{x_i}^{x_{i+1}} \frac{\partial \phi}{\partial x} dx$$

$$= \frac{\overline{\partial \phi}}{\partial x}\Big|_{i+\frac{1}{2}} \stackrel{Eq.(11)}{=} \frac{\partial \overline{\phi}}{\partial x}\Big|_{i+\frac{1}{2}}.$$
(12)

Remark 1 This result suggests that the actual filter length when computing the face derivative is $h_{i+\frac{1}{2}}$, i.e. the distance between the adjacent nodes i and i+1 (see Figure 2).

Finally, the diffusive term in a FVM framework is computed as follows

$$\frac{\partial}{\partial x} \left(\Gamma \frac{\partial \phi}{\partial x} \right) \Big|_{i} \approx \frac{1}{h_{i}} \left(\Gamma \frac{\partial \phi}{\partial x} \Big|_{i+\frac{1}{2}} - \Gamma \frac{\partial \phi}{\partial x} \Big|_{i-\frac{1}{2}} \right)$$

$$= \frac{\partial}{\partial x} \left(\Gamma \frac{\partial \phi}{\partial x} \right) \Big|_{i}$$

$$\approx \frac{1}{h_{i}} \left(\Gamma_{i+\frac{1}{2}} \frac{\phi_{i+1} - \phi_{i}}{h_{i+\frac{1}{2}}} - \Gamma_{i-\frac{1}{2}} \frac{\phi_{i} - \phi_{i-1}}{h_{i-\frac{1}{2}}} \right)$$

$$= \frac{\partial}{\partial x} \left(\Gamma \frac{\overline{\partial \phi}}{\partial x} \right) \Big|_{i}.$$
(13)

In the case of non-constant diffusivity, $\Gamma(x)$, the evaluation of the previous expression can be viewed as filtering the Γ field, *i.e.*

$$\Gamma_{i+\frac{1}{2}} \approx \frac{\Gamma_i + \Gamma_{i+1}}{2} \approx \frac{1}{h_{i+\frac{1}{2}}} \int_{x_i}^{x_{i+1}} \Gamma(x) dx = \overline{\Gamma}_{i+\frac{1}{2}},$$
(14)

while using the trapezoidal rule to approximate the integral. Altogether leads to

$$\frac{\partial}{\partial x} \left(\Gamma \frac{\partial \phi}{\partial x} \right) \Big|_{i} \approx \frac{1}{h_{i}} \left(\frac{\Gamma_{i+1} + \Gamma_{i}}{2} \frac{\phi_{i+1} - \phi_{i}}{h_{i+\frac{1}{2}}} - \frac{\Gamma_{i} + \Gamma_{i-1}}{2} \frac{\phi_{i} - \phi_{i-1}}{h_{i-\frac{1}{2}}} \right) = \frac{\overline{\partial}}{\partial x} \left(\overline{\Gamma} \frac{\overline{\partial \phi}}{\partial x} \right)^{FV} \Big|_{i}, \tag{15}$$

where $\overline{(\cdot)}^{FV}$ is the FVM filtering along the cell i whereas the other two filters are applied to the face quantities and their associated filter lengths are $h_{i+\frac{1}{2}}$ and $h_{i-\frac{1}{2}}$, respectively.

Remark 2 This result suggests that two filtering operations are performed when computing the diffusive term: the calculation of the face derivative (see Eq.12) and the cell-to-face interpolation of the diffusivity (see Eq.14). Both filtering operators share the same filter length; namely, the distance between the nodes adjacent to the corresponding face.

Consequently, this suggests that the SGS characteristic length used to compute the eddy viscosity, ν_t , at the face $i+\frac{1}{2}$ should be $h_{i+\frac{1}{2}}$ (see Figure 2). This concept forms the foundation of this work and can be easily extended to general meshes.

3 Rational length scale

The subgrid characteristic length, δ , appears in a natural way when we consider the calculation of the ν_t at the cell faces. The flowchart displayed in Figure 3 shows that it basically consists on firstly computing the $\hat{\nu}_{t,c}$ at the cells without considering any characteristic length, then interpolating this quantity to the

Figure 3: Flowchart for the implementation of the $\delta_{\rm rls}$. Dashed lines represent the modifications required respect to the usual flowchart.

faces, $\hat{\nu}_{t,s} = \Pi \hat{\nu}_{t,c}$, where Π is a cell-to-face interpolation. Finally, this quantity at the face is re-scaled by the square of the cell distances contained in the diagonal matrix Δ_s (see Trias et al. (2024) for details regarding the construction of Ω_c , Π and Δ_s). Therefore, from an implementation and conceptual point-of-view, the new approach $\delta_{\rm rls}$ (rls stands for rational length scale) is completely different from all previous definitions of δ . Although the required code modifications are minimal (see flowchart in Figure 3), it may be of interest to compute an equivalent length scale that provides the same dissipation. Namely, it can be shown that the local dissipation of the viscous term, with constant viscosity, is given by

$$\nu \mathsf{G} : \mathsf{G} = \nu t r(\mathsf{G}\mathsf{G}^T). \tag{16}$$

If we replace ν by ν_t , we can obtain a very accurate estimation of the local dissipation introduced by an eddy-viscosity model. Furthermore, in the new approach we also need to replace ν_t and G by $\hat{\nu}_t$ and $\hat{\mathsf{G}}$, respectively, leading to

$$\hat{\nu}_t \hat{\mathsf{G}} : \hat{\mathsf{G}} = \hat{\nu}_t tr(\hat{\mathsf{G}}\hat{\mathsf{G}}^T). \tag{17}$$

Then, we can compute an equivalent filter length, $\tilde{\delta}_{\rm rls}$, that leads to the same local dissipation, *i.e.*

$$\tilde{\delta}_{\mathrm{rls}}^{2} \hat{\nu}_{t} \mathsf{G} : \mathsf{G} = \hat{\nu}_{t} \hat{\mathsf{G}} : \hat{\mathsf{G}} \Longrightarrow$$

$$\tilde{\delta}_{\mathrm{rls}} = \sqrt{\frac{\hat{\mathsf{G}} : \hat{\mathsf{G}}}{\mathsf{G} : \mathsf{G}}} = \sqrt{\frac{tr(\hat{\mathsf{G}}\hat{\mathsf{G}}^{T})}{tr(\mathsf{G}\mathsf{G}^{T})}}$$
(18)

where $P_{\mathsf{G}\mathsf{G}^T} = tr(\mathsf{G}\mathsf{G}^T)$ is the first invariant of $\mathsf{G}\mathsf{G}^T$.

4 Numerical results

Isotropic turbulence on anisotropic grids

The novel definitions of the subgrid characteristic length scale, $\delta_{\rm rls}$ and $\tilde{\delta}_{\rm rls}$, respectively proposed in the previous section, are firstly tested for decaying isotropic turbulence. The configuration corresponds to the classical experiment of Comte-Bellot and Corrsin (1971) (hereafter denoted as CBC) using the grid turbulence with a size of M=5.08cm and a freestream velocity $U_0=10m/s$. The Taylor micro-scale Reynolds number at $tU_0/M=42$ (initial state) is $Re_\lambda=u_{rms}\lambda/\nu=71.6$ with $u_{rms}=22.2cm/s$ and decreases to 60.6 at $tU_0/M=171$ (third stage).

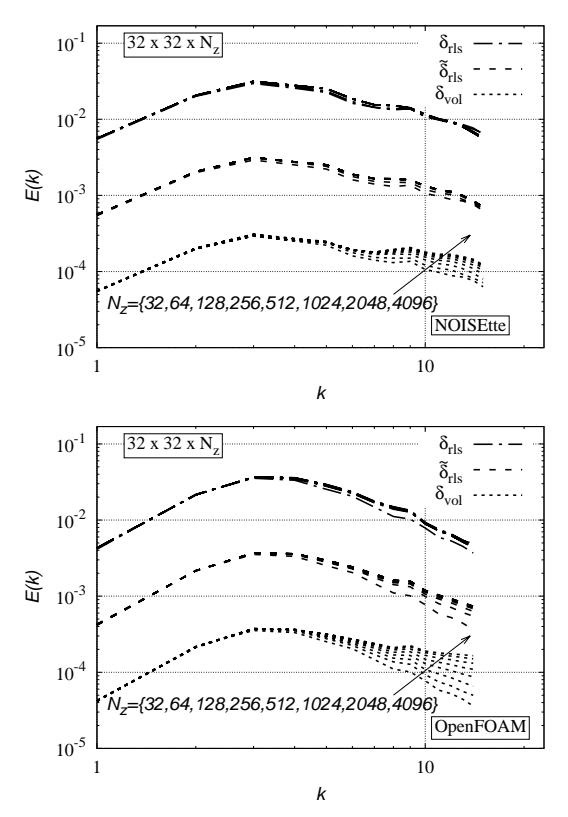


Figure 4: Energy spectra for decaying isotropic turbulence corresponding to the Comte-Bellot and Corrsin (1971) experimental set-up. LES results were obtained using the Smagorinsky model on a set of anisotropic meshes with pancake-like control volumes, employing two different codes: the in-house NOISEtte code (top) and OpenFOAM (bottom). Results obtained with the novel definitions of $\delta_{\rm rls}$ and $\tilde{\delta}_{\rm rls}$ respectively are compared with the classical definition proposed by Deardorff. For clarity, the results obtained with $\tilde{\delta}_{\rm rls}$ and $\delta_{\rm vol}$ are shifted down one and two decades, respectively.

The results are non-dimensionalized with the reference length $L_{ref}=11M/(2\pi)$ and reference velocity $u_{ref}=\sqrt{3/2}u_{rms}|_{tU_0/M=42}$. The energy spectrum of the initial field at $tU_0/M=42$ matches the CBC experimental data. All subsequent results are presented at $tU_0/M=98$, which corresponds to the second stage of the CBC experimental data. Simulations were carried out using two codes: the inhouse NOISEtte solver (see Gorobets and Bakhvalov (2022); Abalakin et al. (2024)) and OpenFOAM. The full setup, including all files required to reproduce the OpenFOAM results, is publicly available in Ruano (2025). In both cases, initial fields were generated by interpolating a $64\times64\times64$ mesh with an energy spectrum corresponding to the CBC initial spectrum.

LES simulations were carried out on a set of artificially stretched meshes using the Smagorinsky model with $C_S=0.17$ (NOISEtte) and $C_S=0.21$ (Open-FOAM), calibrated on a $32\times32\times32$ mesh and kept constant thereafter. Figure 4 shows results for

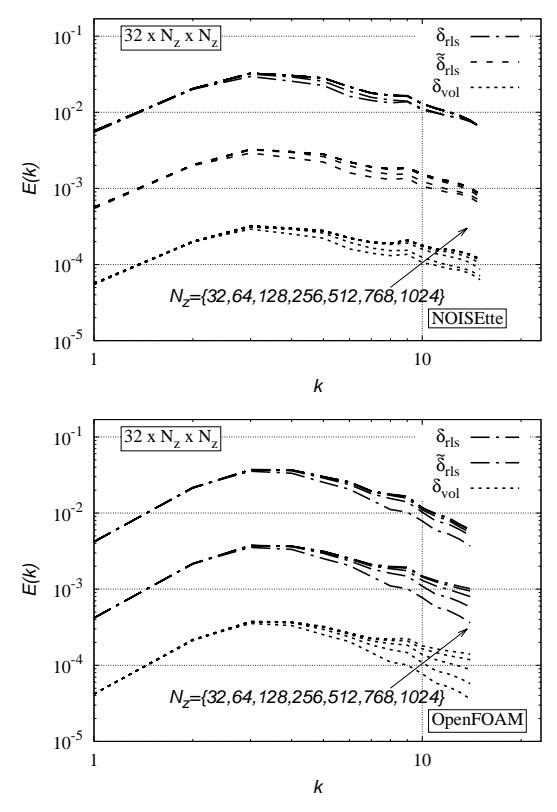


Figure 5: Same as Figure 4 but for pencil-like meshes.

pancake-like meshes of size $32 \times 32 \times N_z$, where $N_z = \{32, 64, 128, 256, 512, 1024, 2048, 4096\}$. As expected, the classical Deardorff definition (see Eq. 4) leads to results that tend to diverge as N_z increases, as $\delta_{\rm vol}$ vanishes, disabling the SGS model. In contrast, the proposed $\delta_{\rm rls}$ and $\tilde{\delta}_{\rm rls}$ definitions yield stable results that quickly converge with mesh refinement. These trends, observed for both codes, suggest that they effectively reduce the influence of mesh anisotropies on the SGS model performance.

A similar trend is observed in Figure 5 for pencillike meshes composed of $32 \times N_z \times N_z$ grid cells, where $N_z = \{32, 64, 128, 256, 512, 768, 1024\}$. In this case, $\delta_{\rm vol}^2$ scales as $\mathcal{O}(\Delta z^{4/3})$ compared to the $\mathcal{O}(\Delta z^{2/3})$ scaling for the pancake-like meshes, causing the eddy-viscosity model (see Eq.2) to switch off even more quickly for increasing values of N_z . Moreover, in this case, the numerical artifact affects a wider range of wavenumbers, whereas for pancakelike meshes, the impact is mostly confined to the smallest resolved scales (see Figure 4). In contrast, LES results obtained with $\delta_{\rm rls}$ and $\delta_{\rm rls}$ show convergence with increasing resolution. However, the first three meshes, i.e. $N_z = \{32, 64, 128\}$, exhibit larger variations than in the pancake case, likely because pencil-like meshes refine two directions, capturing more physical scales and reducing SGS model influence. Overall, the proposed length scales mitigate anisotropy-induced artifacts and offer improved convergence compared to the Deardorff's definition, $\delta_{\rm vol}$.

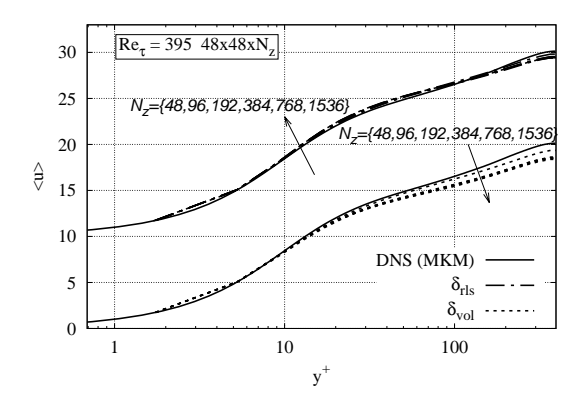
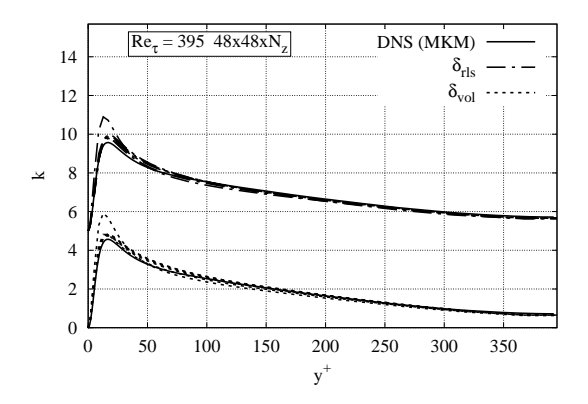


Figure 6: Mean velocity for a turbulent channel flow at $Re_{\tau}=395$ obtained for $48\times48\times N_z$ with $N_z=\{48,96,192,384,768,1536\}$. Solid lines corresponds to the DNS by Moser et al. (1999). LES results obtained using the novel definition, $\delta_{\rm rls}$, are compared against those using $\delta_{\rm vol}$, both employing the S3QR model by Trias et al. (2015a). For clarity, the former results are shifted up.



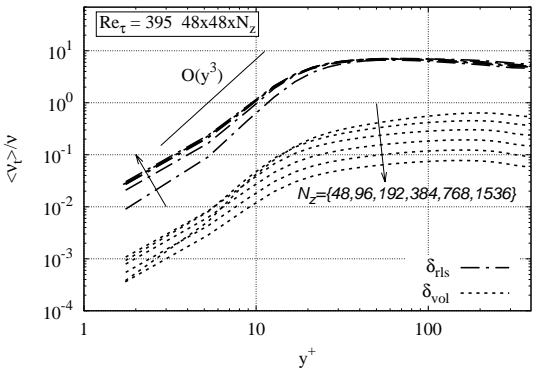


Figure 7: Same as in Figure 6 but for turbulent kinetic energy (top) and the ratio between average turbulent viscosity and the molecular viscosity (bottom).

Turbulent channel flow

To evaluate the performance of the proposed length scale $\delta_{\rm rls}$ in wall-bounded flows, we consider a turbulent channel at $Re_{\tau}=395$. For clarity, only $\delta_{\rm rls}$, which outperformed other alternatives including $\tilde{\delta}_{\rm rls}$, is compared against the standard $\delta_{\rm vol}$. Simulations were performed using a symmetry-preserving staggered finite-volume discretization (see Verstappen and

Veldman (2003)) with the S3QR model by Trias et al. (2015a), as the Smagorinsky model fails to reproduce the near-wall scaling, *i.e.* $\nu_t \propto y^3$. It reads

$$\nu_t^{S3QR} = (C_{s3qr}\delta)^2 Q_{\mathsf{GG}^T}^{-1} R_{\mathsf{GG}^T}^{5/6}, \tag{19}$$

where $C_{s3qr} = 0.762$, Q_{GG^T} and R_{GG^T} are the second and third invariants of the second-order tensor GG^T .

Figure 6 shows the average velocity profiles obtained for a set of (artificially) refined meshes in the span-wise direction, with resolutions of $48 \times 48 \times N_z$ and $N_z = \{48, 96, 192, 384, 768, 1536\}$. This direction was chosen due to its lower sensitivity compared to the stream-wise and wall-normal directions. The domain size matches that of the DNS by Moser et al. (1999), with uniform stream-wise and span-wise grids, and wall-normal points distributed as

$$y_j = \sinh(\gamma j/N_y)/\sinh(\gamma/2) \qquad j = 0, 1, \dots, N_y/2.$$
(20)

with $\gamma=7$. For $N_y=48$, the first off-wall point is located at $y^+\approx 1.75$, and the mesh near the wall is highly anisotropic.

As already observed in the homogeneous isotropic turbulence test-case, the results in Figure 6 confirm that the new definition of $\delta_{\rm rls}$ exhibits significantly greater robustness to mesh anisotropy: the mean velocity profile remains nearly unchanged across refinements, while significant deviations appear with $\delta_{\rm vol}$. A similar trend is observed in Figure 7 (top) for the resolved turbulent kinetic energy, especially in the bulk region where $\delta_{\rm rls}$ displays minimal dependence on N_z .

Finally, Figure 7 (bottom) shows the ratio between the time-averaged turbulent viscosity, $\langle \nu_t \rangle$, and the molecular viscosity, ν , illustrating key differences in SGS activity. With $\delta_{\rm rls}$, this ratio remains consistent as N_z increases, while $\delta_{\rm vol}$ exhibits a pronounced decay in the bulk, effectively deactivating the model. In the near-wall region, both approaches capture the expected cubic scaling, i.e. $\nu_t \propto y^3$, though noticeable differences persist with mesh refinement. Notably, $\delta_{\rm rls}$ leads to a monotonic and rapid convergence of $\langle \nu_t \rangle$, whereas $\delta_{\rm vol}$ does not.

In summary, the channel flow test demonstrates that $\delta_{\rm rls}$ provides consistent predictions for mean velocity, turbulent kinetic energy and turbulent viscosity across a wide range of anisotropic meshes. Unlike $\delta_{\rm vol}$, which is highly sensitive to refinement, $\delta_{\rm rls}$ maintains SGS model activity and accuracy, confirming its suitability for LES in wall-bounded flows.

5 Conclusions

This work addresses a central research question in LES modeling: can we establish a simple, robust, and easily implementable definition of δ for any type of grid that minimizes the impact of mesh anisotropies on the performance of SGS models for LES? Despite its known limitations on highly anisotropic meshes, the Deardorff definition, $\delta_{\rm vol}$, which consists on the

cube root of the cell volume (Eq. 4), remains the most widely used in both research and industry. This motivates the development of improved alternatives.

In this context, we propose the rational length scale $\delta_{\rm rls}$, which arises naturally from the entanglement between LES filtering and numerical discretization. It is locally defined, frame-invariant, well-bounded (see properties P1 and P2 in Table 1), computationally efficient (P6), applicable to unstructured meshes (P4), and evaluated at cell faces (P5), a key feature distinguishing it from existing definitions (see Table 1). Implementation requires only minor changes to standard eddy-viscosity models (see Figure 3), and although derived within a second-order FVM framework, the concept is compatible with other discretization approaches. Moreover, we also introduce the dissipationequivalent definition $\delta_{\rm rls}$ (see Eq. 18), evaluated at cell centers and dependent on the local velocity gradient $G \equiv \nabla \overline{u} (P3).$

The effectiveness of $\delta_{\rm rls}$ and $\tilde{\delta}_{\rm rls}$ has been confirmed through LES of decaying isotropic turbulence using two different codes. Compared to Deardorff's $\delta_{\rm vol}$, both demonstrate significantly greater robustness to mesh anisotropy. Among them, $\delta_{\rm rls}$ consistently performs better in highly stretched configurations. This behavior has also been validated in a turbulent channel flow at $Re_{\tau}=395$, further supporting its practical relevance. Given these results, along with its simplicity, we believe the proposed length scale has strong potential for application in SGS models, particularly in complex geometries involving highly anisotropic or unstructured meshes.

Finally, the choice of turbulent length scale is also crucial in hybrid RANS–LES methods, particularly DES. As shown in the previous work by Pont-Vílchez et al. (2021), even models with strong grey-area mitigation properties may fail in regions of resolved turbulence on anisotropic meshes. This is especially relevant in aeroacoustic applications (see Duben et al. (2023), for instance), where poor resolution of turbulence dynamics can significantly degrade predictions. The proposed $\delta_{\rm rls}$ thus emerges as a promising candidate for use in DES simulations as well.

Acknowledgments

F.X.T. and J.R. are supported by SIMEX project (PID2022-142174OB-I00) of the *Ministerio de Ciencia e Innovación* MCIN/AEI/10.13039/501100011033 and the European Union Next GenerationEU. Calculations were carried out on the MareNostrum 5-GPP supercomputer at BSC. We thankfully acknowledge these institutions.

References

Abalakin, I., Bakhvalov, P., Bobkov, V., Duben, A., Gorobets, A., Kozubskaya, T., Rodionov, P., and Zhdanova, N. (2024). NOISEtte CFD&CAA Supercomputer Code for Research and Applications. Supercomputing Frontiers and Innovations, 11(2):78 – 101.

- Comte-Bellot, G. and Corrsin, S. (1971). Simple Eulerian time correlation of full- and narrow-band velocity signals in grid-generated, isotropic turbulence. *Journal of Fluid Mechanics*, 48:273–337.
- Dabbagh, F., Trias, F. X., Gorobets, A., and Oliva, A. (2020). Flow topology dynamics in a three-dimensional phase space for turbulent Rayleigh-Bénard convection. *Physical Review Fluids*, 5:024603.
- Deardorff, J. W. (1970). Numerical study of three-dimensional turbulent channel flow at large Reynolds numbers. *Journal of Fluid Mechanics*, 41:453–480.
- Deck, S. (2012). Recent improvements in the Zonal Detached Eddy Simulation (ZDES) formulation. *Theoretical and Computational Fluid Dynamics*, 26(6):523–550.
- Duben, A., Ruano, J., Gorobets, A., Rigola, J., and Trias, F. X. (2023). Evaluation of enhanced gray area mitigation approaches based on jet aeroacoustics. *AIAA Journal*, 61(2).
- Gorobets, A. and Bakhvalov, P. (2022). Heterogeneous CPU+GPU parallelization for high-accuracy scale-resolving simulations of compressible turbulent flows on hybrid supercomputers. Computer Physics Communications, 271:108231.
- Mockett, C., Fuchs, M., Garbaruk, A., Shur, M., Spalart, P.,
 Strelets, M., Thiele, F., and Travin, A. (2015). Two Nonzonal Approaches to Accelerate RANS to LES Transition of Free Shear Layers in DES. In Girimaji, S., Haase, W., Peng, S.-H., and Schwamborn, D., editors, *Progress in Hybrid RANS-LES Modelling*, volume 130 of *Notes on Numerical Fluid Mechanics and Multidisciplinary Design*, pages 187–201. Springer International Publishing.
- Moser, R. D., Kim, J., and Mansour, N. N. (1999). Direct numerical simulation of turbulent channel flow up to $Re_{\tau}=590$. *Physics of Fluids*, 11:943–945.
- Pont-Vílchez, A., Duben, A., Gorobets, A., Revell, A., Oliva, A., and Trias, F. X. (2021). New strategies for mitigating the Grey Area in DDES models. *AIAA Journal*, 59(9):3331–3345.
- Ruano, J. (2025). DHIT GitHub Page: https://github.com/jruanoperez/DHIT.
- Scotti, A., Meneveau, C., and Lilly, D. K. (1993). Generalized Smagorinsky model for anisotropic grids. *Physics of Fluids A*, 5(9):2306–2308.
- Shur, M. L., Spalart, P. R., Strelets, M. K., and Travin, A. K. (2015). An Enhanced Version of DES with Rapid Transition from RANS to LES in Separated Flows. Flow, Turbulence and Combustion, 95:709–737.
- Trias, F. X., Álvarez-Farré, X., Alsalti-Baldellou, A., Gorobets, A., and Oliva, A. (2024). An efficient eigenvalue bounding method: CFL condition revisited. *Computer Physics Communications*, 305:109351.
- Trias, F. X., Folch, D., Gorobets, A., and Oliva, A. (2015a). Building proper invariants for eddy-viscosity subgrid-scale models. *Physics of Fluids*, 27(6):065103.
- Trias, F. X., Gorobets, A., and Oliva, A. (2015b). Turbulent flow around a square cylinder at Reynolds number 22000: a DNS study. *Computers & Fluids*, 123:87–98.
- Verstappen, R. W. C. P. and Veldman, A. E. P. (2003). Symmetry-Preserving Discretization of Turbulent Flow. *Journal of Computational Physics*, 187:343–368.